Heritable maize microbiomes contribute to local adaptation and host stress resilience

Xiaoming He[1,2,3,#], Danning Wang[2,3,#], Yong Jiang[4,#], Meng Li[5,#], Manuel Delgado-Baquerizo[6,7,#], Chloee McLaughlin[5], Caroline Marcon[3], Li Guo[3], Marcel Baer[3], Yudelsy A.T. Moya[8], Nicolaus von Wirén[8], Marion Deichmann[9], Gabriel Schaaf[9], Hans-Peter Piepho[10], Zhikai Yang[11], Jinliang Yang[11], Bunlong Yim[12], Kornelia Smalla[12], Sofie Goormachtig[13,14], Franciska T. de Vries[15], Hubert Hüging[16], Ruairidh J. H. Sawers[5,*], Jochen C. Reif[4,*], Frank Hochholdinger[3,*], Xinping Chen[1,*], Peng Yu[2,3,*]

[1] College of Resources and Environment, and Academy of Agricultural Sciences, Southwest University (SWU), 400715 Chongqing, P. R. China
[2] Emmy Noether Group Root Functional Biology, Institute of Crop Science and Resource Conservation (INRES), University of Bonn, 53113 Bonn, Germany
[3] Crop Functional Genomics, Institute of Crop Science and Resource Conservation (INRES), University of Bonn, 53113 Bonn, Germany
[4] Department of Breeding Research, Leibniz Institute of Plant Genetics and Crop Plant Research (IPK), 06466 Gatersleben, Germany
[5] Department of Plant Science, Pennsylvania State University, State College, PA 16802, USA
[6] Laboratorio de Biodiversidad y Funcionamiento Ecosistémico. Instituto de Recursos Naturales y Agrobiología de Sevilla (IRNAS), CSIC, Av. Reina Mercedes 10, E-41012, Sevilla, Spain.
[7] Unidad Asociada CSIC-UPO (BioFun). Universidad Pablo de Olavide, 41013 Sevilla, Spain.
[8] Department of Physiology and Cell Biology, Leibniz Institute of Plant Genetics and Crop Plant Research (IPK), 06466 Gatersleben, Germany
[9] Plant Nutrition, Institute of Crop Science and Resource Conservation (INRES), University of Bonn, 53115 Bonn, Germany
[10] Biostatistics Unit, University of Hohenheim, 70599 Stuttgart, Germany
[11] Department of Agronomy and Horticulture, University of Nebraska-Lincoln, NE 68583 Lincoln, United States
[12] Institute for Epidemiology and Pathogen Diagnostics, Julius Kühn-Institut – Federal Research Centre for Cultivated Plants (JKI), Messeweg 11–12, D-38104 Braunschweig, Germany
[13] Department of Plant Biotechnology and Bioinformatics, Ghent University, Ghent, Belgium.
[14] Center for Plant Systems Biology, VIB, Ghent, Belgium.
[15] Institute for Biodiversity and Ecosystem Dynamics, University of Amsterdam, Amsterdam, Netherlands.
[16] Crop Science Group, Institute of Crop Science and Resource Conservation (INRES), University of Bonn, 53115 Bonn, Germany

[#] These authors equally contributed to this work.

[*] To whom correspondence should be addressed:

rjs6686@psu.edu

reif@ipk-gatersleben.de

hochholdinger@uni-bonn.de

chenxp2017@swu.edu.cn

yupeng@uni-bonn.de

Running title: Adaptive advantage of maize against soil microbes

Key words: Adaptation, maize, microbiome, root, rhizosphere

Author contributions

P.Y., X.C. and F.H. designed the study; P.Y. coordinated and managed the whole project; X.H. performed the culture and harvest of the phytochamber experiments. D.W. analysed the microbiome data and performed all statistical analysis; Y.J. and J.C.R., performed the genetic analysis; C.Mc. and R.J.H.S. performed machine learning and environmental genome-wide association analysis; M.D.B. performed ecological analysis; B.Y. and K.S. contributed bacterial strains from maize; X.H. and M.B. performed bacterial inoculation experiments; X.H. and L.G. extracted all the DNA samples; M.L., Z. Y. and J. Y performed the genomic prediction analysis; P.Y. and H-P P. discussed and designed the large pot experiment; C.Ma. and F.H. contributed the Mu-transposon induced lines; M.D., G.S., Y.A.T.M. and N.v.W. conducted the soil and plant nutrient analyses. S.J.S. and H.H. performed the preparation of soil from Dikopshof long-term experimental station; X.H., D.W., Y.J., M.L., M.D.B., R.J.H.S., J.C.R., X.C., F.H. and P.Y. wrote the paper. All authors read and approved the final version of the manuscript.

Abstract

Beneficial interactions with microorganisms are pivotal for plant adaptation and fitness. Yet, the adaptive trajectories and genetic mechanisms underlying plant-microbiome interactions remain elusive. Here, we surveyed the root and rhizosphere microbiome of 129 accessions of *Zea mays*, sourced from diverse habitats and grown under control and different stress conditions. We demonstrate the impact of domestication and local adaptation on heritable variation in microbiome assembly. Plant genotype and native environment were predictive of the microbiome composition, and the microbiome itself was correlated with plant fitness. Combining microbiome and environmental properties identified host genetic variants linked to rhizosphere microbiome variation with respect to their native habitats. We functionally characterized a gene that controls lateral root formation and mediates association with a keystone microbe, linked to growth promotion and biomass heterosis. We conclude that genetic variation in traditional crop varieties contributes to optimizing the adaptation of the microbiome to local constraints, which bears implications for breeding resilient cultivars.

Main

Microorganisms that colonize the rhizosphere surrounding plant roots, root surfaces and internal tissues play a pivotal role in regulating plant health and fitness under biotic and abiotic stresses[1,2]. Nevertheless, the genetic basis of how host plants control the composition of their root microbiome under optimal or stress conditions remains poorly understood. This critical gap of knowledge remains for two reasons. First, we do not understand the degree to which plants can establish and maintain key microbiomes to ensure plant fitness under particular stress conditions. For example, legumes can develop specified root structures in association with rhizobia to support keystone microbiomes. Yet, whether cereal crops developed strategies to accommodate less well-known microbes with a similar impact on plant performance and resilience remains virtually unknown. Second, we lack comprehensive studies investigating the influence of heritable root traits in driving crop microbiomes. The reason is that the influence of crop species on microbiomes is often exclusively investigated in isolation for a particular crop variety without considering the vast immensity of trait variation across crop varieties and domestication status. Optimization of the crop microbiome has been proposed as a long-term route to promoting food security, while supporting a healthy environment[3,4]. Domesticated plants, in particular locally adapted traditional varieties ("landraces"), provide a powerful resource to investigate the contribution of crop microbiomes to local adaptation across diverse, and often challenging environments[5-8]. During domestication plants have developed resilience to environmental constraints, but may have also lost beneficial microbiome-associated traits compared with their wild relatives[9,10]. Maize (*Zea mays.* L) is an excellent model for investigating the genetic basis of environmental adaptation due to the extensive climatic variation across its original habitats[11,12]. Understanding the genetic basis of how host plants control the composition of their microbiome is critical to reduce the chemical footprint of agriculture and to promote crop resilience to various abiotic stresses that are likely to increase in future climate scenarios.

Heritable variation is detected in the maize microbiome under abiotic stresses

We used 16S rRNA gene and ITS gene sequencing to characterize the root and rhizosphere microbiome of 129 *Zea* accessions, across a wide range of maize and teosinte varieties of distinct domestication status, aiming at investigating the impact of plant genotype and local adaptation on crop-microbiome associations and their capacity to influence plant fitness under common stress conditions. These analyses included 11 teosinte, 97 landrace, 11 maize inbred line and 10 maize hybrid accessions (Supplementary Fig. 1) grown in control-, low phosphorous-, low nitrogen-, and drought-exposed soils to simulate different levels of nutrient and water stress (Supplementary Fig. 2). We sampled root and rhizosphere compartments from 1st shoot-borne crown roots (Supplementary Fig. 3), in addition to collecting bulk soil. Microbial community composition differed across samples for both bacteria and fungi, with compartment explaining the largest proportion of the variation followed by stress treatment (Fig. 1a). Although plant genotype was less important than either compartment or treatment, there was still significant heritable variation associated with both bacterial and fungal microbiomes (Fig. 1b). In the rhizosphere and roots, we observed significantly lower bacterial diversity under drought stress and nitrogen deficiency compared to control conditions (Supplementary Fig. 4a). In contrast, no significant differences in bacterial community diversity were observed between phosphorus deficient and control conditions (Supplementary Fig. 4a). For fungal diversity, the only significant treatment difference was observed between nitrogen deficiency and control conditions in both the rhizosphere and the root (Supplementary Fig. 4b). These results illustrate greater sensitivity under abiotic stresses of maize-associated bacterial than of fungal communities, while the variation of plant genotype has a small but significant heritable impact on microbiome assemblage[13-15], more so under abiotic stresses.

Keystone genera define the major differences in the microbiome

Keystone microbial taxa are defined as the drivers of microbiome structure and function[16]. We identified putative keystone microbes among the highly abundant amplicon sequence variants (ASVs) using co-occurrence network analysis (Supplementary Datasets 1-4). Overall, the number of associations and accumulative weights of ASVs were largely positive within the bacterial or fungal networks, but negative in the inter-kingdom network (Supplementary Fig. 5; Supplementary Dataset 5). This is consistent with previous reports that inter-kingdom interactions determine the overall assembly, stability, and fitness of the root microbiome in *Arabidopsis*[17]. We also observed that a high proportion of the negative inter-kingdom associations were conserved across the stress treatments (Supplementary Fig. 5c; Supplementary Dataset 6). For example, keystone taxa in the bacterial genera *Massilia*, *Sphingobium* and *Streptomyces* were conserved across the stress treatments (Supplementary Fig. 6). Functional prediction indicates that these bacterial genera are involved in ureolysis (*Massilia*) and aerobic chemoheterotrophy (*Sphingobium* and *Streptomyces*) (Supplementary Dataset 7). Keystone fungal

taxa were mainly decomposers and pathogens (Supplementary Dataset 8). Overall, our co-occurrence network analyses revealed strong negative correlations between bacterial and fungal ASVs in roots, while keystone bacterial members are important in microbiome assemblage and stability regardless of abiotic stress treatment. Thus, bringing back keystone and microbiome related traits from wild relatives as well as broader crop diversity may contribute to adaptation of crops to future challenges of climate change.

The impact of plant genotype on the rhizosphere bacterial community increases under stress

To estimate the influence of the plant genotype on microbiome composition, we estimated the correlation between the plant genetic distance matrix and the microbiome distance matrix, for both root and rhizosphere. There was a significant correlation between the bacterial communities and plant genotypes in both compartments. In contrast, fungi displayed a significant correlation with the plant genotype only in the rhizosphere (Supplementary Fig. 7). We estimated the broad-sense heritability (H^2) for the microbiome at different taxonomic levels and for individual ASVs across the experiment and then separately for each compartment and treatment combination (Supplementary Dataset 9; see methods). Plant genotype explained a small but significant proportion of variation in the microbiome compared with compartment or treatment (Supplementary Fig. 8). Across treatments, H^2 was higher for the rhizosphere than the root at the level of families (Fig. 1b), genera (Supplementary Fig. 9a) or ASVs (Supplementary Fig. 9b). Nutrient stress increased H^2 for the bacterial microbiome, but not of the fungal microbiome. In particular, the bacterial taxon *Oxalobacteraceae* under nitrogen limitation showed the highest H^2 among all families in our experiment (Supplementary Fig. 10). *Oxalobacteraceae* have been previously proposed to play an important role in maize resilience when grown in nitrogen-deficient soils[18]. To identify plant genetic loci affecting microbiome composition, we performed genome-wide association (GWA) analysis for all heritable ($H^2 > 0.1$) microbial traits (Supplementary Dataset 10). We did not recover significant markers in association with overall measures of microbial alpha-diversity (Shannon index). We did, however, identify significant associations with individual ASVs (Supplementary Dataset 11). The number of significant associations increased 1.5-3 times from the rhizosphere to the root microbiome (Supplementary Fig. 11), consistent with overall estimates of H^2. Our genetic and environmental analyses support the hypothesis that the genetic constitution of the host shapes microbiome assembly in crops[19-23]. Furthermore, our work highlights the importance of ecological and genetic factors driving plant-microbe interactions in favour of local adaptation. Collectively, these data indicate an increasing impact of the plant genotype on microbiome composition, especially the composition of the rhizosphere bacterial community under stress, consistent with a role of the microbiome in plant adaptation to local environmental constraints.

Plant source habitats predict the root and rhizosphere microbiome

To further address the hypothesis that plant control of soil microbes plays a role in local adaptation, we assessed the potential of the environment at the point of collection of local varieties to predict the microbiome in our standardized growth chamber experiments. For each plant accession, we compiled soil and climatic descriptors from public databases (see methods) corresponding to the point of collection (Supplementary Fig. 1; Supplementary Dataset 12). To reduce the complexity of the microbiome data, we applied Spearman correlation analysis and defined four microbial assemblies corresponding to the respective dominant ASVs (Supplementary Figure 12). We then sought evidence of covariation among microbial assemblies and environmental descriptors (Supplementary Figure 13). We used structural equation modeling to quantify the cumulative effects of source environment, plant genetic diversity, stress treatment, domestication status and biomass on the four microbial assemblies. These analyses demonstrated the impact of plant genotype and source environment on specific assemblies of microbial communities. Low nitrogen treatment, source mean annual temperature, source precipitation and plant genotype strongly impacted the microbiome assemblage (Supplementary Figure 14), one notable example being the abundance of the genus *Massilia*, which belongs to the previously mentioned *Oxalobacteraceae* (Supplementary Figure 15). We then investigated the potential of plant genotype and environmental descriptors to predict microbiome composition. Overall, prediction was better for bacterial data than for fungal data, and better for rhizosphere than root (Fig. 2a; Supplementary Fig. 16). Interestingly, microbiome composition could be predicted more accurately with environmental descriptors or a combination of these with plant genetic markers than with genetic markers alone (Fig. 2a; Supplementary Fig. 17−19). Our combined ecological modelling and prediction analyses indicate that genetic differentiation across plant source environments impacts the microbiome, notably the composition of rhizosphere bacterial communities, consistent with local adaptation of maize to key climate and soil properties. Therefore, plant-microbe associations depend on the match between partner genotypes and bacterial adaptation to their local host[24,25], thus supporting the notion that the impact of the genotype on microbial hubs contributes to host fitness across environments[26].

Consideration of the rhizosphere bacterial community improves prediction of plant fitness traits

Although environmental conditions were dominant drivers of the crop microbiome, we also found certain microbial taxa that were consistently influenced by genetic variability in maize, and whose abundance correlated with plant fitness. To assess the importance of the microbiome for plant performance, we used a two-step strategy combining genomic prediction and Random Forest models based on environmental descriptors. First, we evaluated the H^2 of fitness-related phenotypes including biomass, leaf area, leaf chlorophyll content (measured by SPAD) and nitrogen and phosphorus concentration (Supplementary Figure 20). The average H^2 of all nutrient traits was 0.45 under control conditions rising to a maximum of 0.53 for the low nitrogen treatment (Supplementary Dataset 13). Despite moderately high H^2 values, the only associations we obtained in GWA analysis for our fitness traits were for biomass (Supplementary Datasets 14 and 15). Next, we explored the ability to predict fitness-related phenotypes using microbiome ASVs abundance data alone or in combination with plant genotype. The combination of plant genotype and rhizosphere bacterial community composition provided the highest average prediction ability and the largest prediction coverage across all fitness traits (Fig. 2b; Supplementary Datasets 16 and 17). We confirmed this result employing an alternative approach to fit a ridge regression mixed model, observing greater prediction accuracy when using both genetic and microbiome data (Supplementary Figure 21). As has been previously seen in foxtail millet[23], we showed a conserved pattern that the rhizosphere microbiome combined with genotype data increased the prediction accuracy of agronomic traits compared to genetic markers alone (Supplementary Figure 22). We then explored relationships among source environments, genetic differentiation and specific microbial taxa. As a measure for the pattern of similarity among samples, we calculated matrices of pairwise distance using the observed microbiome ASVs in different treatments, and two source environmental descriptors (*elevation* and *geographical distance*). Mantel tests were used to study the correlations between different distance matrices. We observed that the correlation between the rhizosphere microbiome and source environment was higher than that between the root microbiome and environment. On average, the correlations of inter-treatment and treatment-environment similarity patterns as characterized by bacterial communities were higher than by fungal communities (Supplementary Fig. 23). To reduce dimensionality, we extracted the first five principal components (PCs) from the microbiome ASV data. We then used a Random Forest (RF) approach to predict these PCs using different environmental descriptors as explanatory variables (Supplementary Dataset 12). We observed the highest accuracy for the rhizosphere bacteria PC2 (Supplementary Fig. 24a) using environmental predictors including *photosynthetically active radiation* and *potential evapotranspiration* (Supplementary Fig. 24b). Prediction of individual ASVs was less successful (Supplementary Fig. 25), although significant predictors were identified for specific examples belonging to the *Oxalobacteraceae*, including *Massilia* (Supplementary Fig. 26). These results suggest that plant genetic variation linked to source environment drives variation in the microbiome composition with an impact of plant fitness. Rhizosphere microbiome variation explains microbial diversity along a broad range of temperatures and water availabilities, supporting the increasing functional importance of the rhizosphere under harsh environments[27] and as a heritable trait across environments[28]. We report here a significant advantage for plant trait prediction when combining rhizosphere microbiome with plant genetic data, which highlights the potential utility of the rhizosphere microbiome in breeding stress-resilient crops.

A candidate gene linked to the source environment associates with *Oxalobacteraceae* and root branching

To identify loci associated with variation in the microbiome and differences in source environment, we used our RF models to predict microbiome ASVs for 1781 genotyped traditional varieties on the basis of associated source environmental descriptors and subsequently implemented GWA analyses (Fig. 3a). One of the best predictions (RF model $R^2 = 0.28$) was for root abundance of ASV37, belonging to the genus *Massilia*, in the low nitrogen treatment, consistent with our previous estimates of H^2. Collectively, GWA hits from environmental predictions of AS37 abundance for the 1781 panel overlapped more than expected by chance with the hits from the observed ASV37 data in the smaller 129 panel (Supplementary Fig. 27). The top GWA hit for predicted ASV37 root abundance under low nitrogen (SNP S4_10445603) fell within the gene Zm00001d048945 on chromosome 4 (Fig. 3a and b; Supplementary Dataset 18). Across the 1781 panel, the minor allele at SNP S4_10445603 was more abundant at higher predicted ASV37 abundance but lower source soil nitrogen content (Fig. 3c). These findings are consistent with a specific gene contributing to the geographical adaptation to nitrogen-poor soil by facilitating enhanced association with *Massilia*[18] (Supplementary Fig. 28). The gene Zm00001d048945 is most strongly expressed in the root cortex (Fig. 3d; https://www.maizegdb.org/gene_center/gene/Zm00001d048945) and is predicted to encode a TPX2 domain containing protein related to the WAVE-DAMPENED2 microtubule binding protein that functions

in *Arabidopsis* root development[29] and lateral root initiation[30]. Using root architectural data available for the 126 panel, we found a positive correlation between lateral root density and ASV37 abundance (r = 0.2, P = 0.03; Fig. 3e). To test the hypothesis that variation in Zm00001d048945 contributes to a root-architecture-related effect on ASV37, we identified transposon insertional mutants in two different genetic backgrounds (B73 and F7; Supplementary Fig. 29). Plants homozygous for transposon insertions in Zm00001d048945 showed a significant reduction in lateral root density (Fig. 3f and g). During maize domestication and improvement, the root system expanded its functionality and complexity[31,32]. We interpret these results as evidence that variation at Zm00001d048945 contributes to local adaption by optimizing root traits and recruitment of specific microbes in low nitrogen soils. Notably, we found that potentially environment-adaptive alleles may explain microbiome-driven nitrogen deficiency tolerance and root trait differentiation. These results provide strong support for a genetic basis for variation in the abundance of the bacterial taxon *Massilia* (*Oxalobacteraceae*) under nitrogen deficiency, illustrating the importance of specific bacteria for root development[33], nitrogen acquisition[34] and reciprocal interaction[18]. We conclude that plants have evolved to overcome abiotic stresses by interacting with specific microbial taxa and adjusting their rhizosphere microbiome to nitrogen availability.

The bacterial keystone taxon *Oxalobacteraceae* contributes to maize biomass heterosis

To explore further the effect of root-microbe interactions on maize tolerance to low nitrogen, we focused more broadly on the *Oxalobacteraceae,* which contains the genus *Massilia* and have previously been characterized to be important under nitrogen limitation[18] (Fig. 3). GWA analyses demonstrated that the abundance of *Massilia* ASVs ASV37 and ASV49 can be explained at high probability by marker-trait associations (Sum R^2 = 0.52 and 0.28, respectively), while significant associations were also identified in presence/absence GWA analysis for ASV49 (Fig. 4a; Supplementary Dataset 19). Recent studies highlighted that recruitment of the maize rhizosphere microbial community has been substantially impacted by both domestication[35,36] and modern hybrid breeding[37,38]. Modern breeding is accompanied by progressive habitat changes with the use of pesticides and fertilizers to promote high yields and to protect domesticated crops from biotic and abiotic stress factors despite the risk of adverse effects on the establishment of beneficial microbial associations[39]. To this end, we explored the genetic potential of microbiome optimization in crop breeding based on the heterosis for microbiome traits (Fig. 4b), finding that soil microbes differentially impact the early growth of inbred and hybrid maize[40]. We tested mid-parent heterosis of individual ASVs using FDR-corrected *t*-tests of their variance-stabilized abundances. Here the heterosis of individual ASVs was defined with respect to mid-parent values. In most crossing triplets, the majority of the rhizosphere bacterial ASVs showed some evidence of mid-parent heterosis, however the prevalence of ASV heterosis varied among hybrids for different taxa (Fig. 4b; Supplementary Dataset 20). Specifically, *Oxalobacteraceae* abundance showed heterosis in the rhizosphere of B73 × H99, B73 × H84, B73 × A554 and B73 × Mo17 (Fig. 4b). To characterize the relationship between growth heterosis and abundance of *Oxalobacteraceae* or the specific *Massilia* ASV37, we performed root inoculation experiments. We inoculated with ASV37 alone, with a 17-member synthetic bacterial community (SynCom) of *Oxalobacteraceae* that did not include ASV37 (*Duganella*, *Pseudoduganella*, *Collimonas* and *Janthinobacterium*), or with an 18-member SynCom including the 17-members with the addition of ASV37. We quantified root and shoot growth in inbred lines and hybrids in both nitrogen-rich and nitrogen-poor soil. We found that *Oxalobacteraceae* were important to maintain the growth of hybrids irrespective of soil nitrogen levels, but only necessary for growth of inbred lines under nitrogen-poor soil (Supplementary Figure 30). Moreover, when we compared the degree of mid-parent heterosis for shoot dry biomass, absence of *Oxalobacteraceae* were important to promote heterosis in nitrogen-poor soil (Fig. 4c), thus suggesting that growth of inbred parents might depend more on *Oxalobacteraceae* than hybrids. Furthermore, we verified that different SynComs or single ASV inoculation of *Massilia* ASV37 can significantly induce lateral root formation in both inbred lines and hybrids under nitrogen-poor conditions (Supplementary Figure 31). In particular, we found that heterosis for lateral root density correlated tightly with that in shoot biomass under nitrogen-poor conditions (Fig. 4d). Significantly, the microbial hub taxon *Massilia* alone can contribute to heterosis for lateral roots and biomass of maize, indicating the potential value of root trait interactions with keystone microbial taxa when breeding for crop resilience.

Conclusions

Our study advances the current understanding of plant-microbiome-environment interactions by demonstrating that local adaptation and domestication can govern assembly, dynamics and stability of bacterial hub members and functional capabilities of the maize microbiome in diverse environmental habitats. Beneficial associations between maize and the local soil microbiome could have played a role in plant survival and reproduction during historical expansion to new environments. Understanding how

313 plants modulate the microbiome to help them to adapt to local environments and how this is encoded
314 in the genetic program provides novel insights into establishment of beneficial host–microbiome
315 associations. This knowledge is crucial to harnessing the crop microbiome to support food production
316 and will facilitate the identification of environment-tailored cultivars recruiting favourable microbial
317 consortia for increasing agricultural productivity, resilience to climate change and sustainability.

Online Methods

Plant material, soil collection and growth conditions

The germplasm used in this study was selected to represent a broad diversity ranging from the maize progenitor teosinte to local open pollinating landraces and modern inbred lines and hybrids (Supplementary Dataset 21; Supplementary Fig. 1). We obtained the 11 geographically diverse teosinte accessions from the North Central Regional Plant Introduction Station (NCRPIS) and the International Maize and Wheat Improvement Center (CIMMYT). Moreover, we received the 97 landrace accessions from NCRPIS and these accessions were derived from the ten American countries which cover the major domestication areas of maize (Supplementary Fig. 1a). The modern breeding germplasm includes seven genetically diverse inbred lines[41] covering the major heterotic groups stiff-stalk and non-stiff stalk and four additional tropical inbred lines (Supplementary Fig. 1b). We have produced the ten hybrids by crossing the ten inbred lines with the reference inbred line B73 as the common mother plant (Supplementary Fig. 1c). Soil used for phytochamber pot experiments was dug from the Dikopshof long-term fertilizer field experiment established in 1904 near Cologne, Germany (50˚48′21″N, 6˚59′9″E) (Supplementary Fig. 2a). In this study, we collected soil subjected to three different fertilization managements including control soil fertilized with all nutrients, low nitrogen soil fertilized without nitrogen and low phosphorus soil fertilized without phosphorus as defined accordingly[42]. The general soil type is classified as a Haplic Luvisol derived from loess above sand. Approximately the first 0-20 cm of the soil were collected and placed in a clean plastic bag. Subsequently, collected soil was dried at room temperature in clean plastic trays for about one week and sieved with a 4 mm analytical sieve (Retsch, Haan, Germany) to remove stones and vegetative debris. The sieved soil for the whole experiment was then homogenized with a MIX125 concrete mixer (Scheppach, Ichenhausen, Germany) (Supplementary Fig. 2a). The air-dried soil was ground into powder for the analysis of carbon, nitrogen, phosphorus and five metal elements (K, Fe, Mn, Cu, Zn). Soil pH was measured in deionized water (soil: solution ratio, 1:2.5 w/v) using a pH-meter 766 (Knick, Berlin, Germany). The basic physical and chemical properties of these soils are provided in Supplementary Table 1.

Local landraces are open-pollinated varieties and can vary largely on seed traits. Therefore, we covered a broad geographic area but also confirmed the homogeneity of the 97 landraces concerning seed size, seed color, and seed quality prior our phytochamber experiments (Supplementary Fig. 2b). Seeds were surface-sterilized with 6% NaClO for 10 min, and rinsed 3 times with sterile deionized water to eliminate any seed-borne microbes on the seed surface. The sterilized seeds were pre-germinated for 3 days in a paper roll system using germination paper (Anchor Paper Co., St. Paul, MN, USA) with sterile deionized water. Then seedlings with primary roots of ca. 1–2 cm length were transferred to soil-filled pots (7 × 7 × 20 cm^3) in a 16/8-h light/dark, 26/18 °C cycle and were grown for 4 weeks in a walk-in phytochamber. A detailed sowing and transfer plan is provided in Supplementary Fig. 2c. No additional fertilizer was added.

Experimental design and treatments

The experiment was performed in a split plot design with three replications comprising four stress treatments on the main plots (trays) (Supplementary Fig. 32), e.g. fully fertilized control (CK) soil, no nitrogen fertilized low nitrogen (LN) soil, no phosphorus fertilized low phosphate (LP) and CK soil with drought (D) treatment. As controls, we used six pots without plants as ‘bulk soil’ samples (B), which were distributed across the main plots. Each tray contained a similar number of pots (subplots) with the different genotypes and bulk soil. The three replicates were performed at three different periods in the same growth chamber (Supplementary Fig. 32). For each stress treatment, we generated an alpha design for the genotypes and controls with three replicates and four incomplete blocks per replicate. The incomplete blocks were assigned to trays and replicates corresponded to the three replications of the experiment in time. To facilitate watering, pots subjected to the same treatment were allocated on the same tray. These trays were further randomized in the chamber. Distribution of all pots in each tray were randomized using a true random generator (excel function “RAND”), and trays were reshuffled every week in the growth chamber without paying attention to the pot labels. Since soil water availability will significantly affect the harvest of the rhizosphere and initiation of crown roots, we have performed a preliminary experiment with different water regimes (i.e. 33%, 22%, 17% water holding capacity) to ensure the establishment of suitable drought conditions and to facilitate rhizosphere harvesting and the optimal formation of the different whorls of crown roots (Supplementary Fig. 2c and 33). In brief, different volumes of sterilized water e.g. 60 ml, 40 ml, 30 ml were mixed with 500 g dry soil by spraying water and were then homogenized with a 4 mm sieve (Retsch). Each water regime was maintained by spraying water to the soil surface according to the weight loss of water during the 4-week culture. Plant height, total leaf area, shoot and root fresh biomass from the representative genotypes B73 and Mo17

were recorded. Moreover, the multifunctional device COMBI 5000 (STEP Systems, Nuremberg, Germany) was used to measure soil variables e.g. soil moisture and electronic conductivity directly in each soil pot during each experimental run. The covariates including sample harvest time, ID of person performing DNA extraction together with the determined soil variables were collected and used for downstream data analysis (Supplementary Dataset 22).

Characterization of native collection sites of maize landraces

Geographical coordinates and elevation information of the collection sites for maize landraces were retrieved from the public database of the U.S. National Plant Germplasm System (https://www.grin-global.org/) and provided in Supplementary Dataset 21. Most of the landraces were received in the years 1980-1994 and were maintained by NCRPIS. To get the climate and soil variables based on the geographical coordinates for each site, we first compiled climatic and soil descriptors representative of the long-term averages of their point of origin, following methods accordingly[43]. All used databases are publicly available and have global coverage. Data was collected from WorldClim[44], the NCEP/NCAR reanalysis project (https://psl.noaa.gov/data/reanalysis/reanalysis.shtml)[45], NASA SRB (https://asdc.larc.nasa.gov/project/SRB), Climate Research Unit (CRU)[46], SoilGrids[47] and the Global Soil Dataset (GSD)[48]. All 156 bioclimatic and soil variables were merged with the maize germplasm identity into the Supplementary Dataset 12. The related information of total soil nitrogen, available phosphorus, and annual precipitation are provided in the Supplementary Fig. 34.

Determination of shoot phenotypic traits and ionome profile

Aboveground phenotypic traits were determined for all 129 genotypes on the day of harvest in the phytochamber. The leaf area and chlorophyll index as measured by SPAD were determined as described accordingly[18] and are provided in Supplementary Dataset 23. The complete aboveground part of maize plants excluding the seed was harvested and heat treated at 105 °C for 30 min, dried at 70 °C to constant weight, weighed as the shoot dry biomass and then ground into powder. Approximately 6 mg of ground material was used to determine total nitrogen concentration in an elemental analyzer (Euro-EA, HEKAtech). Data were then calculated into peak areas by the software Callidus, providing quantitative results using reference material as a calibration standard. The same plant material was used to determine the concentrations of 13 additional mineral nutrients. In brief, approximately 200 mg of same ground material was weighed into polytetrafluoroethylene digestion tubes, and concentrated nitric acid (5 ml, 67–69%; Bernd Kraft) was added to each tube. After 4 h of incubation, samples were digested under pressure using a high-performance microwave reactor (Ultraclave 4, MLS). Digested samples were transferred to Greiner centrifuge tubes and diluted with deionized (Milli-Q) water to a final volume of 8 ml. Element analysis was carried out by Inductively Coupled Plasma-Optical Emission Spectroscopy (iCAP 7400 duo; Thermo Fisher Scientific). For sample introduction a SC-4 DX autosampler with prepFAST Auto-Dilution System (ESI, Elemental Scientific) was used. A three-point external calibration curve was set from a certified multiple-standards solution (Custom Multi-Element Standard_PlasmaCAL, S-prep GmbH). The element Yttrium (ICP Standard Certipur®, Merck) was infused online and used as internal standard for matrix correction. All ionome data including concentrations and contents of all mineral nutrients are provided in the Supplementary Dataset 24.

Root and rhizosphere samples harvest for microbiome analysis

The root and rhizosphere samples collection were performed from 4-week-old maize plants as previously described[18]. In brief, whole root systems were carefully taken out from each pot and vigorously shaken to remove all soil not firmly attached to the roots. During this stage, most genotypes have consistently started to form the 2nd whorl of shoot-borne crown roots with a length of 3-10 cm. To synchronize the harvest for precise comparisons among genotypes, we collected the fully developed 1st whorl of shoot-borne crown roots initiated from the coleoptilar node for all maize genotypes (Supplementary Fig. 6a). Two dissected crown roots with tightly attached soil were placed into a 15 ml Falcon (Sarstedt) tube and immediately frozen in liquid nitrogen and stored at -80 °C before extraction of rhizosphere soil. The rhizosphere samples were defined and extracted into PowerBead tubes (Mo Bio Laboratories) as described previously[18]. The root samples were harvested from another crown root from the same plant that immediately washed by tap water and rinsed with three times of sterilized water followed by tissue drying and placed in PowerBead tubes (Supplementary Fig. 6b). Sample processing steps for root and rhizosphere have been performed by a designated person to avoid systematic errors. The bulk soil samples were also collected from the unplanted pots. DNA extractions were performed soon after root and rhizosphere samples were harvested, following the PowerSoil DNA isolation kit (Mo Bio Laboratories) protocol.

Amplicon library preparation and sequencing

Amplicon library construction was processed with a similar workflow as previously described[18] (Supplementary Fig. 6c). In brief, for bacterial 16S rRNA gene libraries, the V4 region was amplified using the universal primers F515 (5′ GTGCCAGCMGCCGCGGTAA 3′) and R806 (5′ GGACTACHVGGGTWTCTAAT 3′)[49]. For fungal amplicon sequencing, the *ITS1* gene was amplified by the primer pair F (5′ CTTGGTCATTTAGAGGAAGTAA 3′) and R (5′ GCTGCGTTCTTCATCGATGC 3′). PCR reactions were performed with Phusion High-Fidelity PCR Master Mix (New England Biolabs) according to the manufacturer's instructions. Subsequently, only PCR products with the brightest bands at 400-450 base pairs (bp) were chosen for library preparation. Equal density ratios of the PCR products were mixed and purified with the Qiagen Gel Extraction Kit. Sequencing libraries were generated using the NEBNext Ultra DNA Library Pre Kit for Illumina, following the manufacturer's recommendations and with the addition of sequence indices. The library quality was checked on a Qubit 2.0 Fluorometer (Thermo Scientific) and Agilent Bioanalyzer 2100 system. Finally, the qualified libraries were sequenced by 250-bp paired-end reads on a MiSeq platform (Illumina).

16S rRNA gene and ITS gene sequence processing

Raw sequencing reads were processed following a similar workflow as previously described[18]. Briefly, paired-end 16S rRNA amplicon sequencing reads were assigned to samples based on their unique barcode and truncated by cutting off the barcode and primer sequence. Paired-end reads were merged using FLASH (v1.2.7)[50] and the splicing sequences were called raw tags. Sequence analyses were performed by QIIME 2 software (v2020.6)[51]. Raw sequence data were demultiplexed and quality filtered using the q2-demux plugin followed by denoising with DADA2[52] (via q2-dada2). Sequences were truncated at position 250 and each unique sequence was assigned to a different ASV. Taxonomy was assigned to ASVs using the q2-feature-classifier[53] and the classify-sklearn naïve Bayes taxonomy classifier against the SSUrRNA SILVA 99% OTUs reference sequences (v138)[54] at each taxonomic rank (kingdom, phylum, class, order, family, genus, species). Mitochondria- and chloroplast-assigned ASVs were eliminated. Out of the remaining sequences (only features with >10 reads in ≥2 samples) were kept to build an ASV table. In order to study phylogenetic relationships of different ASVs, multiple sequence alignments were conducted using mafft (via q2-alignment)[55] and the phylogenetic tree was built using fasttree2 (via q2-phylogeny)[56] in QIIME 2. Those sequences that did not align were removed. ITS amplicon data were processed the same as 16S amplicon data except that used the UNITE 99% ASVs reference sequences (v10.05.2021)[57] to annotate the taxonomy.

Statistical analyses for microbial community assembly

In consideration of experimental design, here we treated the trays as the main plots for different treatments as a random effect. There were four trays per period/replicate, and a replicate effect was considered to account for differences between the three replicates. All downstream analyses were performed in R (v4.1.0)[58]. Briefly, ASV tables were filtered with ≥10 reads in ≥2samples. For α-diversity indices, Shannon index was calculated using ASV tables rarefied to 1,000 reads. For all the following analyses ASVs which express ≤0.05% relative abundance within ≤5% samples were filtered. After filtering taxa, the samples with ≤1000 reads were also removed. Bray–Curtis distances between samples were calculated using ASV tables that were normalized using 'varianceStabilizingTransformation' function from DESeq2 (v1.34.0) package[59] in R. Constrained ordination analyses were performed using the 'capscale' function in R package vegan (v2.5-7)[60]. To test the effects of compartment, treatment and genotype on the microbial composition community, variance partitioning was performed using Bray–Curtis distance matrix between pairs of samples with a permutation-based PERMANOVA test using 'adonis' function in R package vegan[60].

Inter-kingdom associations by network analysis

The method SPIEC-EASI (SParse InversE Covariance Estimation for Ecological Association Inference) implemented in SpiecEasi (v1.1.2) R package was used to construct the inter-kingdom microbial associations[61] and network was visualized by Cytoscape (v3.9.1). For this network inference, only ASVs with relative abundance >0.05% in ≥10% samples were used. The filtered bacterial and fungal ASV table were combined as the input followed by the default centered log-ratio (CLR) transformation. The neighborhood selection measured by the Meinshausen and Bühlmann (MB) method[62] was selected as the inference approach. The number of subsamples for the Stability Approach to Regularization Selection (StARS) was set to 99.

Genotyping of 129 maize genotypes

Genomic DNA was extracted from leaves of bulked maize seedlings subjected to different treatments for each genotype (Supplementary Fig. 6). The genetic variation across the maize genotypes was characterized using a GenoBaits Maize40K chip containing 40 K SNP markers, which was developed using a genotyping by target sequencing (GBTS) platform in maize[63]. In brief, DNA fragmentation, end-repair and adding A-tail, adapter ligation and probe hybridization were performed. After ligation of the adapters and clean up, fragment size selection was done with Beckman AMPureBeads and a PCR step to enrich the library. Quantity and quality of the libraries were determined via Qubit™ 4 Fluorometer (Invitrogen) and Agilent 2100 Bioanalyzer, respectively. In total, 129 qualified and enriched libraries were sequenced as 250-400 bp on an MGISEQ-2000 (MGI, Shenzhen, China). The quality of raw sequencing reads was assessed and filtered by fastp (version0.20.0, www.bioinformatics.babraham.ac.uk/projects/fastqc/) with the parameters (-n 10 -q 20 -u 40). The clean reads were then aligned to the maize B73 reference genome v4 using the Burrows-Wheeler Aligner (BWA) (v0.7.13, bio-bwa.sourceforge.net) with the MEM alignment algorithm. The SNPs were then called using the UnifiedGenotyper tool from Genome Analysis Toolkit (GATK, v3.5-0-g36282e4, software.broadinstitute.org/gatk) SNP caller. The genetic distance matrix was calculated based on pairwise Rogers' distance[64]. A principal component analysis (PCA) was performed based on the filtered SNPs by GCTA software[65]. A phylogenetic tree (Supplementary Fig. 35) was generated using the neighbour-joining method as implemented in Mega 10.0.4 with 1,000 bootstraps using MEGA-X[66].

Analyses of phenotypic data

For the three fitness phenotypes (SPAD, leaf area and biomass), we first performed the outlier test using the following model for a given stress treatment:

$$y_{ijk} = \mu + \beta_{t(i)} + g_i + r_j + b_{jk} + e_{ijk}, \quad (1)$$

where y_{ijk} is the observation of the *i*-th genotype in the *k*-th block of the *j*-th complete replicate. μ is the general mean, $\beta_{t(i)}$ is the effect of the *t*(*i*)-th subpopulation (*t*(*i*) indicates the subpopulation that the *i*-th genotype belongs to. There are four subpopulations: teosinte, landraces, inbred lines and hybrids.), g_i is the effect of the *i*-th genotype, r_j is the effect of the *j*-th replicate, b_{jk} is the effect of the *k*-th block nested within the *j*-th replicate and e_{ijk} is the residual term. All effects except the general mean were assumed to be random and follow an independent normal distribution.

After fitting the model, the residuals were standardized by the rescaled median of absolute deviation from the median (MAD) and then a Bonferroni-Holm test was applied to flag the outliers[67].

For all traits including fitness phenotypes and microbial traits, we estimated the broad-sense heritability (also referred as repeatability in this case) in each treatment. The following model was used to estimate the heritability:

$$y_{ijk} = \mu + g_i + r_j + b_{jk} + e_{ijk}, \quad (2)$$

where all notations were the same as in (1).

The heritability was calculated using the following formula:

$$H^2 = \frac{\sigma_g^2}{\sigma_g^2 + \sigma_e^2/R}, \quad (3)$$

where σ_g^2 and σ_e^2 are the estimated genotypic and residual variance, *R* is the number of replications.

The best linear unbiased estimations (BLUEs) of all genotypes for each trait in each treatment were obtained by fitting Model (2) once more, assuming the general mean and genotypic effects are fixed and all other effects are random. All linear mixed models were fitted using the software ASReml-R 4.0[68].

Statistical framework for GWAS

Prior to GWAS, we first performed quality control for the genotypic data. In brief, the missing genotypic values were imputed using the software Beagle 5.2[69]. After imputation, we removed the markers with minor allele frequency (MAF) <0.05. As heterozygous loci were very common in our data set, we also removed markers whose maximum genotype frequency is >0.95. In total, 157,785 SNP markers were used for GWAS. For all traits, GWAS was performed separately for each treatment (i.e., using the BLUEs within the treatment as the response variable). For microbiome ASVs and alpha-diversity traits, only those with a heritability >0.1 were used for GWAS.

A standard "Q+K" linear mixed model[70] was used in GWAS. More precisely, the model is of the following form:

$$\boldsymbol{y} = \boldsymbol{X\beta} + \boldsymbol{m}a + \boldsymbol{g} + \boldsymbol{e}, \quad (4)$$

where $\boldsymbol{y}$ is the *n*-dimensional vector of phenotypic records (i.e. BLUEs within a certain treatment, *n* is the number of genotypes), $\boldsymbol{\beta}$ is the *k*-dimensional vector of fixed covariates including the common intercept and the subpopulation effects. $\boldsymbol{X}$ is the corresponding $n \times k$ design matrix allocating each genotype to the subpopulation it belongs to. a is the additive effect of the marker being tested, $\boldsymbol{m}$ is the *n*-dimensional vector of marker profiles for all individuals. The elements in $\boldsymbol{m}$ are coded as 0, 1 or 2, which is the number of minor alleles at the SNP. $\boldsymbol{g}$ is an *n*-dimensional random vector representing the genetic background effects. We assume that $\boldsymbol{g} \sim N(0, \boldsymbol{G}\sigma_g^2)$, where σ_g^2 is the genetic variance component, $\boldsymbol{G}$ is the VanRaden genomic relationship matrix[71]. $\boldsymbol{e}$ is the residual term and $e \sim N(0, \boldsymbol{I}\sigma_e^2)$, where σ_e^2 is the residual variance component and $\boldsymbol{I}$ is the $n \times n$ identity matrix. After solving the linear mixed model, the marker effect was tested using the Wald test statistic $W = \hat{a}^2/\mathrm{var}(\hat{a})$, which approximately follows a χ^2-distribution with one degree of freedom.

Strictly, the model needs to be fitted once for each marker to get the precise test statistic for each marker. But to reduce the computational load, we implemented a commonly used approximate approach, namely the "population parameters previously determined" (P3D) method[72]. That is, we only fit the model once without any marker effect (the so-called "null model"), and then we fixed the estimated the variance parameters σ_g^2 and σ_e^2 throughout the testing procedure. Then, the test statistic for each marker can be efficiently calculated. GWAS was implemented using R codes developed by ourselves. The variance parameters were estimated by the Bayesian method using the package BGLR[73].

For microbial traits, the significant marker-trait association (MTA) was identified with a threshold of p <0.05 after Bonferroni-Holm correction for multiple test[74]. For fitness phenotypes and alpha-diversity, we used a more liberal threshold of p <0.1 after Benjamini-Hochberg correction[75]. For each trait, the proportion of phenotypic variance explained by each MTA (R^2) was calculated as follows: A liner regression model was fitted with all MTAs identified for the trait under consideration. Then, the sum of squares for each MTA as well as the total sum of squares was calculated by ANOVA. The R^2 for each MTA was estimated as the sum of squares of the MTA divided by the total sum of squares.

GWAS for the presence/absence mode

For microbial traits, we performed in addition a GWAS based on the presence/absence mode (PA-GWAS) in each treatment. Each ASV or taxonomy is considered as present if it is present in more than two replicates (including two). As in the GWAS for abundance, ASVs and taxa with repeatability below 0.1 were filtered out. Those with a presence rate above 95% or below 5% were considered as non-segregated and were also excluded from the analysis. The model for PA-GWAS is a logistic linear mixed model[76]. Briefly, the model can be described as follows.

$$\mathrm{logit}(\boldsymbol{\pi}) = \boldsymbol{X\beta} + \boldsymbol{m}a + \boldsymbol{g}, \quad (5)$$

where $\boldsymbol{X}$, $\boldsymbol{\beta}$, $\boldsymbol{m}$, a and $\boldsymbol{g}$ are the same as in (6). $\boldsymbol{\pi}$ is the vector of conditional probabilities given the covariates, marker effects and the genetic background effects. More precisely, for the *i*-th individual, $\boldsymbol{\pi}_i = P(y_i = 1|\boldsymbol{X}_i, m_i, g_i)$, where y_i is the binary variable indicating the presence (y_i = 1) and absence (y_i = 0), $\boldsymbol{X}_i$ is the *i*-th row of the matrix $\boldsymbol{X}$, m_i is the *i*-th entry of the vector $\boldsymbol{m}$ and g_i is the *i*-th component of the random vector $\boldsymbol{g}$. The logit function is defined as $\mathrm{logit}(x) = \ln(x/(1-x))$.

Similar to the P3D approach, a null logistic linear mixed model $\mathrm{logit}(\boldsymbol{\pi}_0) = \boldsymbol{X\beta} + \boldsymbol{g}$ was fitted using the penalized quasi-likelihood method[77]. The estimated variance components were then fixed throughout the test procedure. A score test was applied to assess the significance of the marker effects.

The PA-GWAS was conducted using the R package GMMAT[76].

Prediction for microbial traits using the genomic data and environmental descriptors

To see the host genetics and microbiome assemblage, Mantel test was first performed between Rogers' genetic distance matrix and microbial composition distance matrix only for landraces. After removing the treatment effect using linear model for normalized microbial abundances, the mean value of the residual for each genotype was used to calculate the Euclidean distance. Spearman correlation method was used in mantel function in R. Permutations = 9999.

Next, we investigated the prediction abilities for all microbial traits within each treatment using both the genomic data and the environmental characters. The following three models were implemented. To eliminate the noise of subpopulation effects, we only used the 97 landraces for this part of analysis.

Model 1 (genomic prediction). We applied the genomic best linear unbiased prediction (GBLUP)[71] which is the most commonly used model in genomic prediction. The model can be described as follows.

$$\boldsymbol{y} = \boldsymbol{X\beta} + \boldsymbol{g} + \boldsymbol{e}, \quad (6)$$

where the notations are the same as in (4). Note that by the use of the VanRaden genomic relationship matrix as the covariance matrix of $\boldsymbol{g}$, it implicitly modeled the additive effects of all markers.

Model 2 (prediction purely based on the environmental characters). In this model, the genetic effects were replaced by the effects of the environmental characters, which were modeled in a similar way to the GBLUP. More precisely, the model has the following form:

$$\boldsymbol{y} = \boldsymbol{X\beta} + \boldsymbol{l} + \boldsymbol{e}, \quad (7)$$

where $\boldsymbol{l}$ is the *n*-dimensional random vector representing the E-determined values for all individuals. We assume that $\boldsymbol{l} \sim N(0, \boldsymbol{\Sigma}\sigma_l^2)$ where σ_l^2 is the corresponding variance component, $\boldsymbol{\Sigma}$ is a covariance matrix. Assuming that $\boldsymbol{L}$ is the $n \times s$ matrix of standardized environmental character records (s is the number of environmental characters), we have $\boldsymbol{\Sigma} = \boldsymbol{LL}'/c$ where c is the mean of all diagonal elements in the matrix $\boldsymbol{LL}'$.

Model 3 (prediction based on both genomics and environmental characters). In this approach, we combined the genomic data and the Es in a multi-kernel model, which is of the following form:

$$\boldsymbol{y} = \boldsymbol{X\beta} + \boldsymbol{g} + \boldsymbol{l} + \boldsymbol{e}, \quad (8)$$

where the notations were inherited from (6) and (7).

The prediction abilities of the above three models were assessed in a leave-one-out cross-validation scenario. That is, each individual was predicted once using a training set consisting of all other individuals. Thus, for each trait the prediction model was fitted *n* times. After we obtained the predicted values of all individuals, the prediction ability was calculated as the correlation between the predicted and observed values. The standard error was estimated using the bootstrap approach[78].

All prediction models were implemented using the R package BGLR[73] and rrBLUP[79].

Prediction for fitness phenotypes using the genomic and microbiome data

We explored the possibility of predicting the three fitness phenotypes and ionome traits in each treatment using the genomic data and microbiomes. As in the last subsection, we focused on the subpopulation of 97 landraces.

Scenario 1 (*prediction based on microbiomes only*). In this scenario, we considered 9 cases, in which the phenotypes were predicted using bacteria in the root sample (BA_RO), in the rhizosphere sample (BA_RH), fungi in the root sample (FU_RO), in the rhizosphere sample (FU_RH), bacteria in both samples (BA), fungi in both samples (FU), both types of microbiomes in the root sample (RO), in the rhizosphere sample (RH), and both types of microbiomes in both samples (ALL). The model can be uniformly described as follows:

$$\boldsymbol{y} = \boldsymbol{1}_n\mu + \sum_{i=1}^{k} \boldsymbol{m}_i + \boldsymbol{e}, \quad (9)$$

where $\boldsymbol{m}_i$ is an *n*-dimensional trait values for all individuals determined by a certain type of microbiome in a specific sample, *k* can be 1 (BA_RO, BA_RH, FU_RO, FU_RH), 2 (BA, FU, RO, RH), or 4 (ALL), other notations are the same as in (8). We assume that $\boldsymbol{m}_i \sim N(0, \boldsymbol{V}_i\sigma_{m_i}^2)$, where $\sigma_{m_i}^2$ is the corresponding variance component, $\boldsymbol{V}_i$ is a covariance matrix derived from the microbiome ASVs. Assuming that $\boldsymbol{M}_i$ is the $n \times t$ matrix of standardized records of microbiome ASVs (t is the number of different ASVs), we have $\boldsymbol{V}_i = \boldsymbol{M}_i\boldsymbol{M}_i'/c_i$ where c_i is the mean of all diagonal elements in the matrix $\boldsymbol{M}_i\boldsymbol{M}_i'$.

Scenario 2 (*prediction based on both microbiomes and genomic data*). In this scenario, the 9 cases in Scenario 1 were combined with genomic data (G_BA_RO, G_BA_RH, G_FU_RO, G_FU_RH, G_BA, G_FU, G_RO, G_RH, G_ALL). The models are of the following form:

$$\boldsymbol{y} = \boldsymbol{1}_n\mu + \boldsymbol{g} + \sum_{i=1}^{k} \boldsymbol{m}_i + \boldsymbol{e}, \quad (10)$$

where the notations were adopted from (8) and (11).

As in the last subsection, the prediction abilities were evaluated in a leave-one-out cross-validation scenario. Prediction models were implemented using the R package BGLR.

Effects of source environmental factors on specific microbial assemblies

To explore the environmental legacy of native habitats in relation to specific microbial variations among landraces, we performed network analyses of rhizosphere and root microbial indicators. We then aimed to understand the connections between bacterial and fungal taxa intimately associated with the microbiome of roots and rhizospheres. To this end, we used the function "multipatt" in the R package indicspecies[80] to identify those microbial phylotypes that were significant indicators of microbial zASVs roots and rhizosphere (i.e., roots, rhizosphere or roots + rhizosphere) compared with bulk soil. We then conducted a correlation network conformed by taxa associated with the root and rhizosphere microbiomes. We calculated all pairwise Spearman correlation coefficients among these microbial taxa and kept all positive correlations. We further identified microbial modules (clusters of taxa highly correlated with each other) using Gephi (https://gephi.org/). We determined the proportion of modules by calculating the standardized (0-1) average of all taxa within each module, so that all taxa equally contribute to each module. This information was then correlated (Spearman) with environmental conditions. Mean annual temperature and precipitation were obtained from the WorldClim database (https://www.worldclim.org/). Other environmental descriptors were determined as explained above. Structural equation modelling (SEM) was conducted to provide a system-level understanding on the direct and indirect associations between environmental factors, the proportion of modules and that of selected taxa from above-explained analyses. Because some of the variables introduced were not normally distributed, we used bootstrap tests in these SEMs. We evaluated the fit of these models using the model χ^2-test, the root mean squared error of approximation and the Bollen–Stine bootstrap test.

Environmentally adaptive loci and microbiome relatedness across abiotic stresses

To determine if the environmentally associated loci are contributing to microbiome adaptation to abiotic stresses, we used a representative set of natural varieties e.g. 97 landraces accessions covering typical geographical range. Prior to analysis, PCA was conducted based on the BLUEs for each treatment and compartment to extract major sources of variance from bacterial and fungal microbial community data. The first five PCs were obtained for downstream analyses. PCA was performed using the prcomp function in R. In addition, we selected 18 individual ASVs belonging to *Oxalobacteraceae* to be predicted by Random Forest models. To improve model accuracy, feature selection was conducted prior to model building to eliminate unimportant or redundant environmental variables by identifying those with significant associations to an outcome variable. The feature selection method Boruta was employed to identify environmental aspects that describe significant variation in the PCs and ASVs using Boruta::boruta() (v7.0.0)[81].

The subset of boruta-identified environmental variables (Supplementary Dataset 12) for each ASV were used for Random Forest model construction. This model works under the expectation that a response variable can be described by several explanatory variables through the construction of decision trees. Thus, each Random Forest model is representative of the non-linear, unique combination of explanatory variables that describe variation in a response variable. Random Forest models were built using RandomForest::randomForest() function under default parameters, 5000 trees were built and one third of the number of explanatory variables were tried at each split[82]. Random Forest models were trained with 80% of the data and validated with the remaining 20% test set. Model success was evaluated with percent error explained, Nash-Sutcliffe efficiency (NSE), mean absolute error (MAE), and mean squared error (MSE). Using constructed Random Forest models, ASVs were predicted for 1,781 genotyped landraces in Mexico. These landraces were genotyped as a part of the Seeds of Discovery project (SeeD).

We conducted genome wide association studies (GWAS) to measure the associations between SNPs of landrace genotypes and predicted microbial traits, as well as the associations between SNPs and the environmental variables used to predict the microbial traits. SNPs were filtered for minor allele frequency >1%. We applied the method as previously described[83], using a linear model to fit the genotypic data and each microbial trait and environmental variable for Mexican landrace accessions. The first five eigenvectors of the genetic relationship matrix were included in the model to control for population structure. To control for the number of false positive tests, we re-calibrated the *p*-values using the false discovery rate (FDR) control algorithm[84] and selected significant SNPs based on the calibrated results. To test if GWA hits based on the prediction is significantly better in capturing top GWA hits of observed data than random, we conducted a permutation test and compared the median p-value of GWA hits of observed data that are around 200kb of the top 100 prediction-based GWA hits and the median p-value of random selected GWA hits based on 10000 permutations.

Association of adaptive alleles with soil nitrogen and co-adapted microbial taxa

To identify whether the microbiome has been locally adapted with environment and maize phenotypes, we performed allelic variation analysis of Zm00001d048945 using an SNP dataset of CIMMYT landraces accessions obtained from a previous study[12]. We extracted the genotypic information of top SNPs of the target gene Zm00001d048945 for all tested landraces. We divided maize landraces into 20 groups based on the total soil nitrogen content (%) of their sampling sites[48]. We calculated the mean total nitrogen, the minor allele frequencies (MAF) of the target SNPs, and the mean predicted ASV abundance for each group of landraces. Pearson correlation was conducted to test the correlations between MAF and total nitrogen content, and between MAF and ASV abundance.

Candidate gene validation by independent transposon insertion alleles

Gene expression for Zm00001d048945 was explored in qTeller (https://qteller.maizegdb.org/), which allows to compare gene expression across different tissues from multiple data sources. Gene expression data was extracted from different organs (seed, root, tassel/silk, internodes and leaf) and specific tissues such as the root meristematic zone, elongation zone, stele and cortex. The gene encoded protein annotation was inferred from UniProt database (https://www.uniprot.org/). We next identified potential loss-of-function mutations by exploring the sequence indexed collection BonnMu[85]. Induced maize mutants of the BonnMu resource derive from Mutator-tagged F_2-families in various genetic backgrounds, such as B73 and F7. We identified two insertion lines, BonnMu-8-D-0170 (B73) and BonnMu-F7-2-F-0598 (F7), harboring insertions 1,264 bp upstream of the start codon ATG and in the second exon of Zm00001d048945, respectively. These two families were phenotyped in paper-roll culture[18] and the seedling plants were scanned using the scanner Expression 12000XL (Epson, Suwa, Japan). Lateral roots were counted and the density was normalized with the measure number of lateral roots per cm length of primary root. Statistical analyses were performed by pair-wise Students *t* test with *F* statistics.

Association of relative abundance of *Massilia* with lateral root density

To understand the relationship between *Massilia* and the formation of lateral roots, root system architecture and morphology of 129 maize genotypes was scanned with an Epson Expression 12000XL scanner. Lateral root density was determined by manual calculation as the number of emerged lateral roots per length (cm) of the main root. The linear correlation was plotted between lateral root density and relative abundance data of *Massilia* ASVs using R (v4.1.0).

Functionally adapted microbial inheritance from inbred lines to hybrids

Patterns of heterosis were tested for variance-stabilized counts of highly abundant and prevalent ASVs (>0.05% relative abundance ≥20% samples) for 11 maize inbred lines and 10 hybrids that were crossed with one common mother inbred line B73 according to established protocols[37]. A linear mixed model was employed to test these ASVs features using lmer function from the lme4 (v1.1.27.1)[86] package in R. In the model, blocks were set as random effects while treatments were set as fixed effects to remove noise. The resulted residuals were then used to test for patterns of heterosis. In brief, the mean values of these residuals in the inbred lines and expected mid-parent values (assuming additive genetic variance) for each hybrid were calculated for each ASV feature. Two-sided statistical *t*-tests were conducted for the null hypothesis that each hybrid's microbiome trait value was equivalent to its respective "mid-parent heterosis". Moreover, "better-parent heterosis" was tested using one-sided *t*-tests to assess whether the hybrid value fell outside the parental range. Significance of both tests were adjusted according to the Benjamini-Hochberg method (adjusted *p* values <0.05)[75].

Synthetic community, root bacterial inoculation and plant fitness assay

To explore heterosis manifestation and effects of *Oxalobacteraceae*, a growth promotion assay by inoculation with a synthetic community of *Oxalobacteraceae* isolates (Supplementary Dataset 25) was performed on three maize inbred lines (H84, B73 and Mo17) and their reciprocal hybrids (B73 × H84, B73 × Mo17 and Mo17 × H84) in both nitrogen-rich and nitrogen-poor soil pots. The natural soil was dug from a natural field at Campus Klein-Altendorf (University of Bonn), then sieved, homogenized and mixed with 50% quartz sand (WF 33, Quarzwerke Weferlingen, Germany) to reduce the nitrogen content of the recipient soil. The soil mixtures were then sterilized and conditioned for one week prior to use. The seed sterilization, isolates preparation, root inoculation and growth assay were done according as previously reported[18]. Different genotypes were grown in the phytochamber (16/8 h light/dark and 26/18 °C) for 6 weeks and plants were harvested, and total root and shoot dry weight were determined. To understand the importance of *Massilia* strains for maize heterosis, we performed another inoculation experiment using the same maize inbred lines and hybrids with different synthetic communities e.g. all *Oxalobacteraceae* isolates, *Oxalobacteraceae* isolates excluding *Massilia* ASV37,

753 only *Massilia* ASV37 isolates under nitrogen-poor condition. All preparations and harvests were
754 performed accordingly[18].

755 **Data availability**

756 All raw maize genotyping data, bacterial 16S and fungal ITS data in this paper were deposited in the
757 Sequence Read Archive (http://www.ncbi.nlm.nih.gov/sra) under the BioProject ID PRJNA889703. The
758 SSUrRNA database from SILVA database (release 138, 2020, https://www.arb-silva.de/) and UNITE
759 database (v8.3, 2021, https://unite.ut.ee/) were used for analysing the bacterial 16S and fungal ITS
760 sequences, respectively. We deposited customized scripts about GWAS analysis in the following
761 GitHub repository: https://github.com/Danning16/MaizeMicrobiome2022. All statistical data are
762 provided with this paper.

Main figures

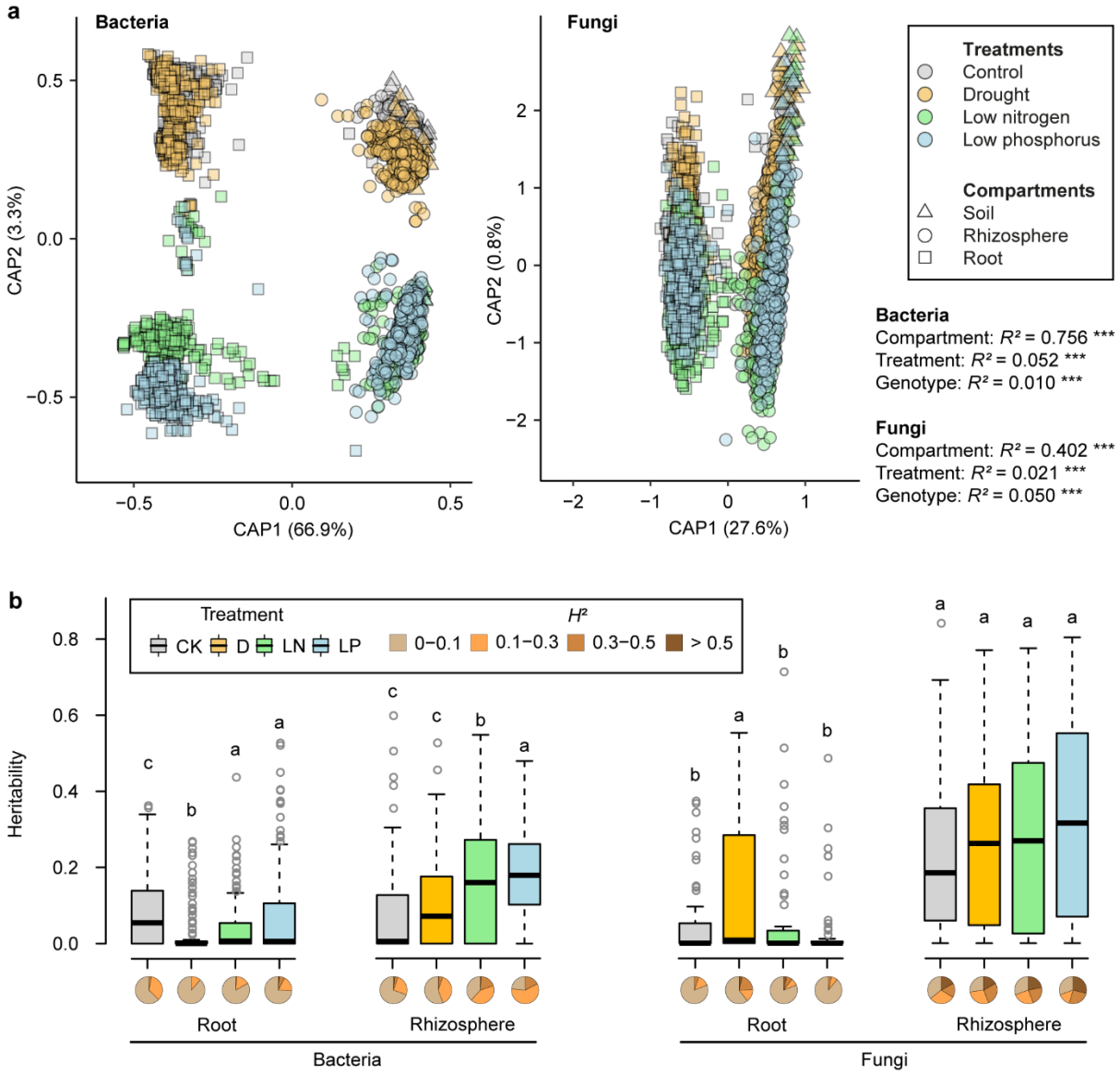

Figure 1. Overall assembly and heritability of microbiome among abiotic stresses. a, Constrained analysis of principle coordinate (CAP) ordination using Bray–Curtis dissimilarity with permutational analysis of variance (PERMANOVA) was applied to visualize significant microbiome differences across three compartments, four treatments and genotypes (n = 129). Datapoints for bacteria (n = 3138) and fungi (n = 3168) are color coded according to the four treatments. Compartments are shape coded. Only ASVs with reads >10 in ≥6 samples were included in the dataset. **b**, Heritability estimates of individual families under four treatments for both bacteria and fungi. The broad-sense heritability (H^2) was calculated using highly abundant bacterial (n = 131) and fungal (n = 59) families across all samples. CK, control; D, drought; LN, low nitrogen; LP, low phosphorus. Significances are indicated among treatment groups for each compartment with Benjamini-Hochberg adjusted P < 0.05 (Kruskal-Wallis test, Dunn's *post-hoc* test). Boxes span from the first to the third quartiles, centre lines represent the median values and whiskers show data lying within 1.5× interquartile range of the lower and upper quartiles. Data points at the ends of whiskers represent outliers. The pie charts indicate the proportional distributions of heritability frequencies.

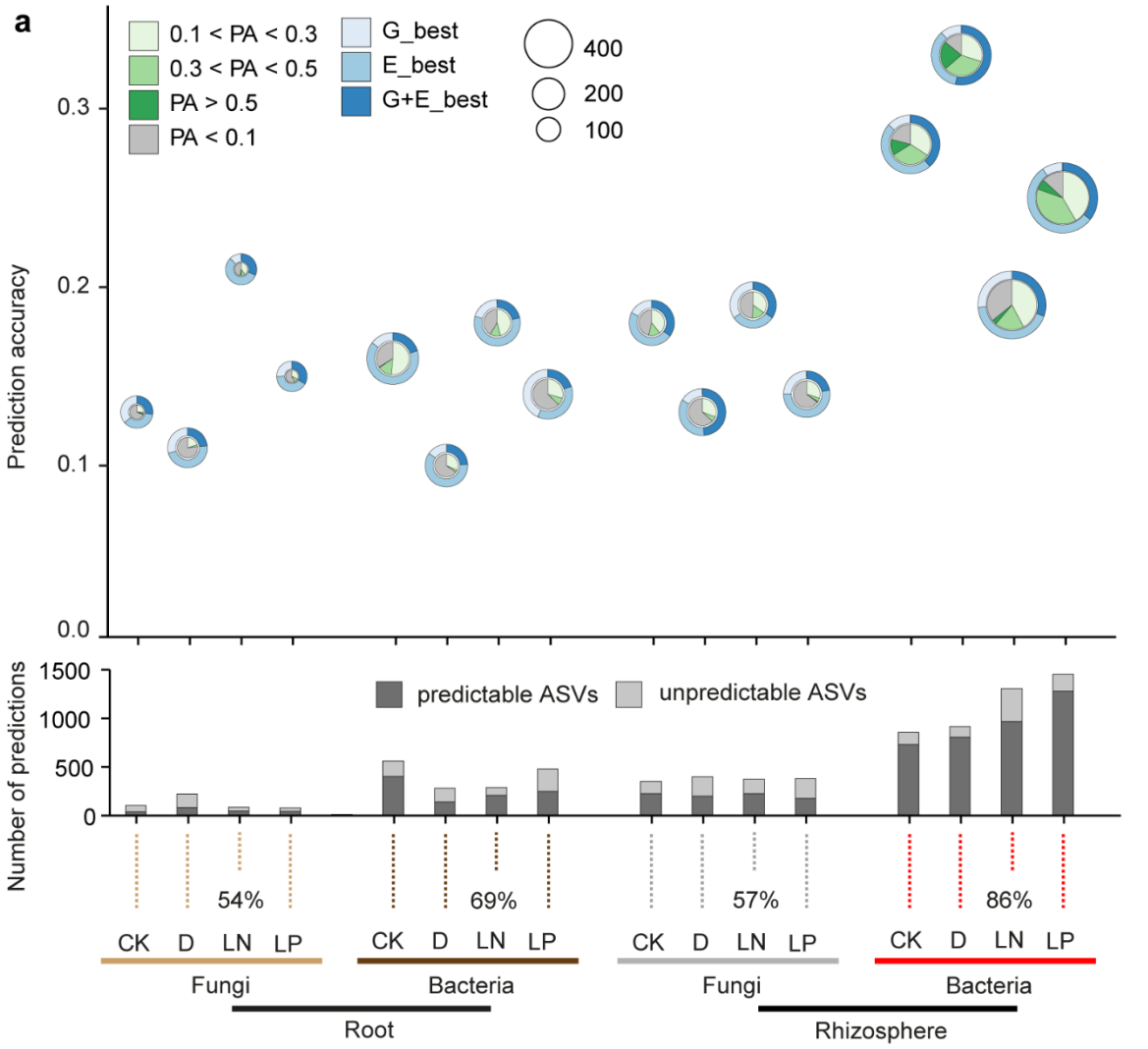

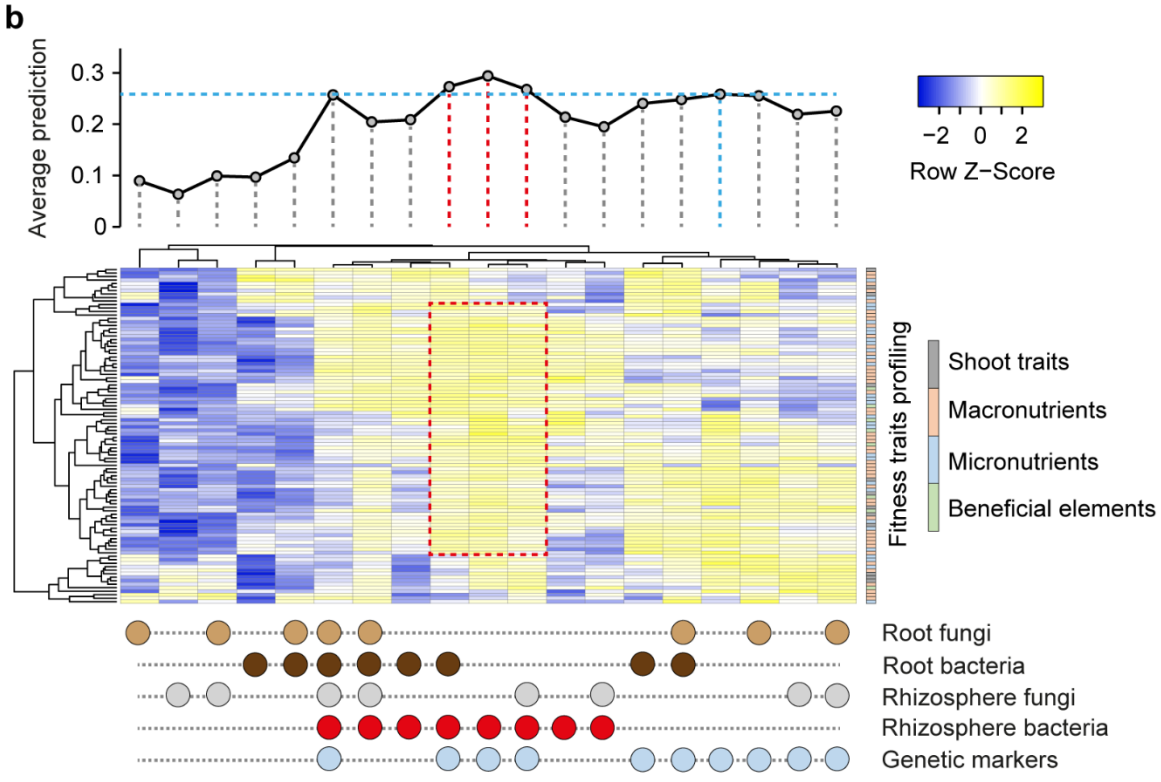

779

Figure 2. Genomic, environmental and microbial prediction of host-microbe interactions and plant fitness. a, Microbiome traits prediction using genetic markers and environmental characters. Inner pie charts describe the proportion of ASVs with four different magnitudes of prediction accuracies from different treatments across compartments. Outer circles define the best prediction patterns observed by applying the genetic markers (G_best) alone, environmental characters (E_best) alone or combined genetic markers and environmental characters (G+E_best). The numbers denote the average prediction accuracies for microbial ASVs from different treatments across compartments. Only ASVs with heritability (H^2) >0.1 were considered in prediction analysis. PA, prediction accuracy. Bar plots indicate the proportions of predictable (PA >0.1) and unpredictable (PA <0.1) ASVs from the total predictions. CK, control; D, drought; LN, low nitrogen; LP, low phosphorus. **b**, Plant fitness traits prediction using genetic markers and microbiome traits. A curved line describes the average prediction accuracy for plant fitness traits using microbiome data alone, genomic data alone or combined genomic and microbiome traits data. A heatmap illustrates the standardized prediction accuracy for fitness traits across different microbiome features combined with genetic markers. Shoot traits include the biomass, leaf area and chlorophyll measured by SPAD value. Nutrient uptake properties include the concentration and content of macronutrients, micronutrients and beneficial elements.

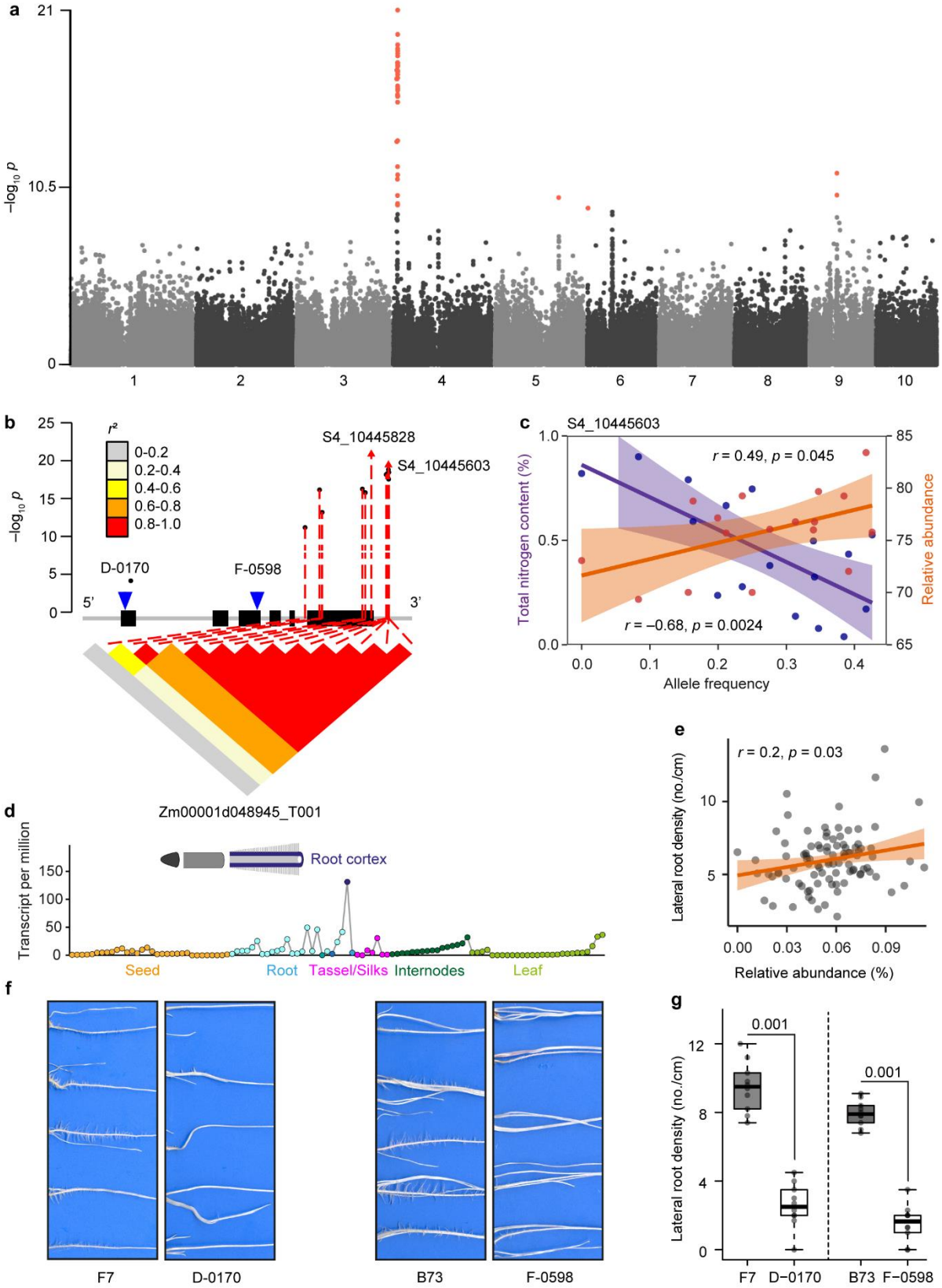

Figure 3. Environmental selection facilitates microbiome-driven root phenotypic co-adaptation to local nitrogen availability. a, Manhattan plots showing environmental GWAS of adaptive of specific *Massilia* ASV37. **b**, Linkage disequilibrium (LD) plot for SNPs within 2.5kb of gene Zm00001d048945. Exons in the gene model are indicated by black bins. All significant SNPs are linked (red) to the LD plot ($P < 1.0 \times 10^{-7}$). Arrows indicate the positions of the peak SNPs. The colour key (grey to red) represents linkage disequilibrium values (r^2). Blue triangles indicate the transposon insertion positions of the two mutant alleles D-0170 and F-0598. **c**, Pearson correlation coefficient analysis of allele frequency

(S4_10445603) with soil total nitrogen content (purple) and predicted relative abundance of ASV37_Root_LN (orange) across 1781 geographical locations worldwide. **d**, Tissue-specific expression of gene Zm00001d048945 according to the eFP Browser database. **e**, Pearson correlation coefficient analysis of lateral root density with relative abundance of ASV37_Root_LN (orange) among 97 maize landraces. Scatter plots show best fit (solid line) and 95% confidence interval (colour shading) for linear regression. **f** and **g**, Root phenotypes and lateral root density of two independent Mu-transposon insertion mutant alleles in comparison to the corresponding wild types (B73 and F7). Significances are indicated between wild type and mutant for different genetic backgrounds (two-tailed Student's *t*-tests). Boxes span from the first to the third quartiles, centre lines represent the median values and whiskers show data lying within 1.5× interquartile range of the lower and upper quartiles. Data points at the ends of whiskers represent outliers.

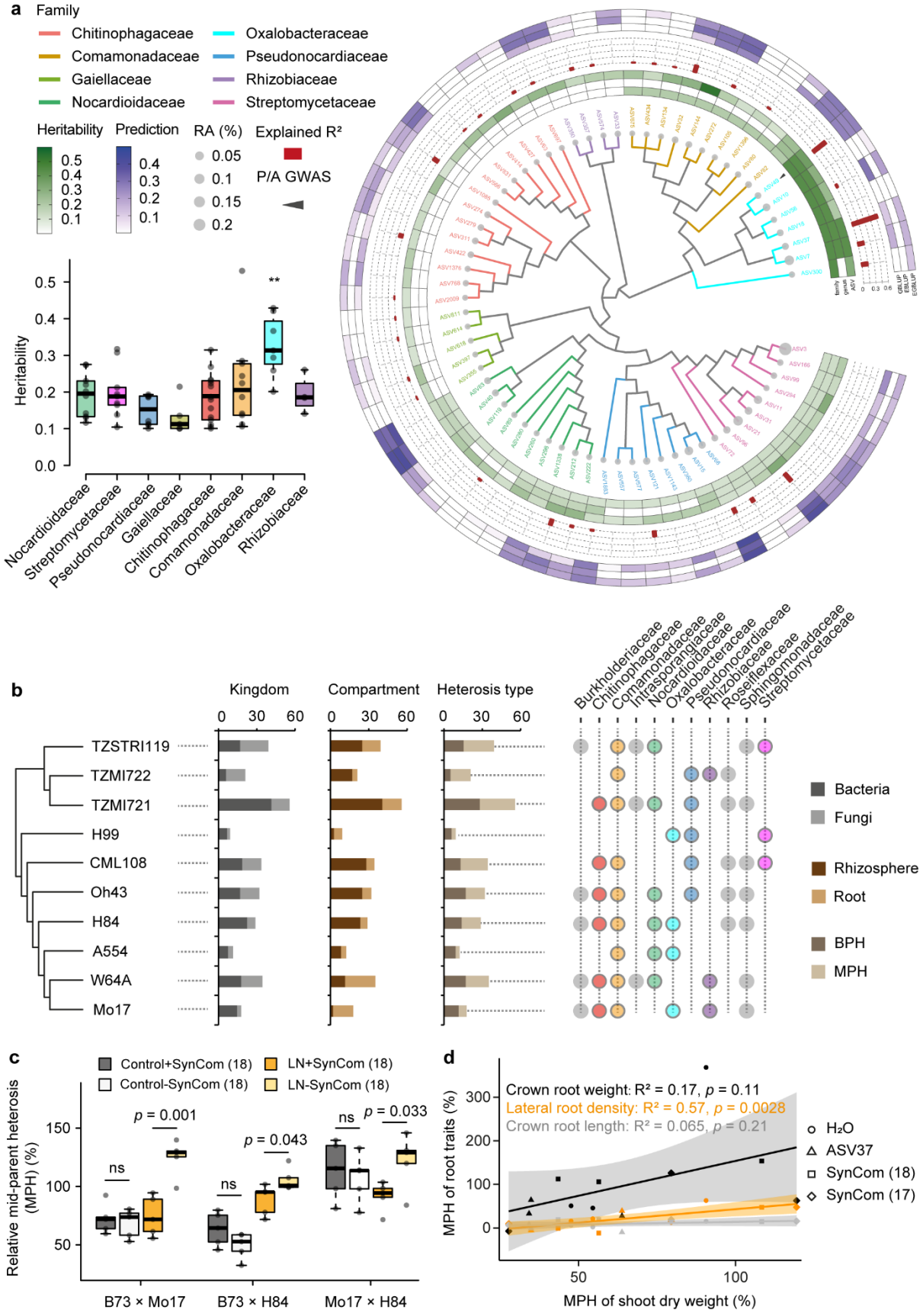

Figure 4. Heterosis confers selective advantage of functional taxa and overall performance under nitrogen deficiency. a, Phylogenetic tree of dominant bacterial ASVs (*n* = 126) of roots grown under nitrogen-poor condition. Dot size corresponds to relative abundance. Inner heatmap from inside

to outside indicates heritability (H^2 >0.1) at the family, genus and ASV level. Red bar plots describe the explained variance by GWAS. The outer heatmap indicates the predictions by genomic best linear unbiased prediction (GBLUP), or based on the environmental best linear unbiased prediction (EBLUP) or prediction based on both genomics and environment (EGBLUP). Triangles indicate significant associations with the presence/absence (P/A) GWAS. Color coded tree branches of ASVs are clustered at the family level. Box plot indicates significantly higher heritability of *Oxalobacteraceae* compared to other families. **b**, Heterosis pattern of microbial ASVs across different crossing triplets. BPH, better parent heterosis; MPH, mid-parent heterosis. Different color-coded dots correspond to the bacterial families described in panel **a**. **c**, MPH of shoot dry biomass in the presence/absence of synthetic *Oxalobacteraceae* communities (SynCom). Significances are indicated in response to presence/absence of SynCom (two-tailed Student's *t*-tests). ns, not significant. LN, low nitrogen. **d**, Correlation between MPH of different root traits and MPH of shoot dry biomass after inoculation with independent soil-derived *Oxalobacteraceae* isolates in nitrogen-poor soil. Scatter plots show combined data from inoculation experiments with best fit (solid line) and 95% confidence interval (color shading) for linear regression.

Acknowledgement

We thank Paul Schulze-Lefert (Max Planck Institute for Plant Breeding Research, Cologne, Germany) for the generous donation of bacterial strains for SynCom experiments. We thank Candice Gardner (United States Department of Agriculture, Ames, US) and the International Maize and Wheat Improvement Center (CIMMYT) for germplasm contribution. We thank Angelika Glogau, for soil and plant nutrient determination and Selina Siemens and Alexa Brox for soil and root DNA extractions (University of Bonn, Bonn, Germany). We thank Yayu Wang and Huan Liu (State Key Laboratory of Agricultural Genomics, BGI-Shenzhen, Shenzhen, China) for providing us the SNP matrix data in foxtail millet. We thank Daliang Ning and Jizhong Zhou (University of Oklahoma, Norman, USA) for suggestions on the microbiome data analysis. This work is supported by Deutsche Forschungsgemeinschaft (DFG) grants HO2249/9-3, HO2249/12-1 to F.H. and YU272/1-1 and Emmy Noether Programme 444755415 to P.Y., the German Excellence Strategy – EXC 2070 – grant 390732324 to P.Y. and G.S., the Bundesministerium für Bildung und Forschung (BMBF) grant 031B195C to F.H. and DFG Priority Program (SPP2089) “Rhizosphere Spatiotemporal Organisation - a Key to Rhizosphere Functions” grant 403671039 to F.H. and P.Y. X.C.’s research is supported by The Changjiang Scholarship, Ministry of Education, China, State Cultivation Base of Eco-agriculture for Southwest Mountainous Land (Southwest University, Chongqing, China), and the National Maize Production System in China (grant no. CARS-02-15).

853 **Main references**

854

855 1. Cheng, Y. T., Zhang, L. & He, S. Y. Plant-microbe interactions facing environmental
856 challenge. *Cell Host Microbe* **26**, 183–192 (2019).
857 2. Oldroyd, G. E. & Leyser, O. A plant's diet, surviving in a variable nutrient environment.
858 *Science* **368**, eaba0196 (2020).
859 3. Singh, B. K., Trivedi, P., Egidi, E., Macdonald, C. A. & Delgado-Baquerizo, M. Crop
860 microbiome and sustainable agriculture. *Nat. Rev. Microbiol.* **18**, 601–602 (2020).
861 4. Trivedi, P., Leach, J. E., Tringe, S. G., Sa, T. & Singh, B. K. Plant-microbiome interactions:
862 from community assembly to plant health. *Nat. Rev. Microbiol.* **18**, 607–621 (2020).
863 5. Meyer, R. S. & Purugganan, M. D. Evolution of crop species: genetics of domestication and
864 diversification. *Nat. Rev. Genet.* **14**, 840–852 (2013).
865 6. Cordovez, V., Dini-Andreote, F., Carrión, V. J. & Raaijmakers, J. M. Ecology and evolution
866 of plant microbiomes. *Annu. Rev. Microbiol* **73**, 69–88 (2019).
867 7. Fitzpatrick, C. R. et al. The plant microbiome: from ecology to reductionism and beyond.
868 *Ann. Rev. Microbiol.* **74**, 81–100 (2020).
869 8. Raaijmakers, J. M. & Kiers, E. T. Rewilding plant microbiomes. *Science* **378**, 599–600
870 (2022).
871 9. Haney, C. H., Samuel, B. S., Bush, J. & Ausubel, F. M. Associations with rhizosphere
872 bacteria can confer an adaptive advantage to plants. *Nat. Plants*. **1**, 15051 (2015).
873 10. de Vries, F. T., Griffiths, R. I., Knight, C. G., Nicolitch, O. & Williams, A. Harnessing
874 rhizosphere microbiomes for drought-resilient crop production. *Science* **368**, 270–274
875 (2020).
876 11. Hake, S. & Ross-Ibarra, J. The natural history of model organisms: genetic, evolutionary
877 and plant breeding insights from the domestication of maize. *eLife* **4**, e05861 (2015).
878 12. Navarro, J. A. R. et al. A study of allelic diversity underlying flowering-time adaptation in
879 maize landraces. *Nat. Genet.* **49**, 476–480 (2017).
880 13. Bulgarelli, D. et al. Revealing structure and assembly cues for *Arabidopsis* root-inhabiting
881 bacterial microbiota. *Nature* **488**, 91 (2012).
882 14. Lundberg, D. S. et al. Defining the core *Arabidopsis thaliana* root microbiome. *Nature* **488**,
883 86 (2012).
884 15. Bulgarelli, D., Schlaeppi, K., Spaepen, S., Van Themaat, E. V. L. & Schulze-Lefert, P.
885 Structure and functions of the bacterial microbiota of plants. *Ann. Rev. Plant Biol.* **64**, 807–
886 838 (2013).
887 16. Banerjee, S., Schlaeppi, K. & van der Heijden, M. G. Keystone taxa as drivers of
888 microbiome structure and functioning. *Nat. Rev. Microbiol.* **16**, 567–576 (2018).
889 17. Durán, P. et al. Microbial interkingdom interactions in roots promote *Arabidopsis* survival.
890 *Cell* **175**, 973–983 (2018).
891 18. Yu, P. et al. Plant flavones enrich rhizosphere Oxalobacteraceae to improve maize
892 performance under nitrogen deprivation. *Nat. Plants* **7**, 481–499 (2021).
893 19. Deng, S. et al. Genome wide association study reveals plant loci controlling heritability of
894 the rhizosphere microbiome. *ISME J.* **15**, 3181–3194 (2021).
895 20. Escudero-Martinez, C. et al. Identifying plant genes shaping microbiota composition in the
896 barley rhizosphere. *Nat. Commun.* **13**, 1–14 (2022).
897 21. Meier, M. A. et al. Association analyses of host genetics, root-colonizing microbes, and
898 plant phenotypes under different nitrogen conditions in maize. *eLife* **11**, e75790 (2022).
899 22. Oyserman, B. O. et al. Disentangling the genetic basis of rhizosphere microbiome
900 assembly in tomato. *Nat. Commun.* **13**, 1–16 (2022).
901 23. Wang, Y. et al. GWAS, MWAS and mGWAS provide insights into precision agriculture
902 based on genotype-dependent microbial effects in foxtail millet. *Nat. Comm.* **13**, 1–17
903 (2022).
904 24. Levy, A. et al. Genomic features of bacterial adaptation to plants. *Nat. Genet.* **50**, 138–150
905 (2018).
906 25. Batstone, R. T., O'Brien, A. M., Harrison, T. L. & Frederickson, M. E. Experimental evolution
907 makes microbes more cooperative with their local host genotype. *Science* **370**, 476–478
908 (2020).
909 26. Brachi, B. et al. Plant genetic effects on microbial hubs impact host fitness in repeated field
910 trials. *Proc. Natl Acad. Sci. USA* **119**, e2201285119 (2022).
911 27. Ramirez, K. S. et al. Detecting macroecological patterns in bacterial communities across
912 independent studies of global soils. *Nat. Microbiol.* **3**, 189–196 (2018).

913 28. Walters, W. A. et al. Large-scale replicated field study of maize rhizosphere identifies
914 heritable microbes. *Proc. Natl Acad. Sci. USA* **115**, 7368–7373 (2018).
915 29. Yuen, C. Y., Pearlman, R. S., Silo-Suh, L., Hilson, P., Carroll, K. L. & Masson, P. H. WVD2
916 and WDL1 modulate helical organ growth and anisotropic cell expansion in Arabidopsis.
917 *Plant Physiol.* **131**, 493–506 (2003).
918 30. Qian, Y., Wang, X., Liu, Y., Wang, X., Mao, T. HY5 inhibits lateral root initiation in
919 Arabidopsis through negative regulation of the microtubule-stabilizing protein TPXL5. *Plant*
920 *Cell* doi: 10.1093/plcell/koac358 (2022).
921 31. Yu, P., Gutjahr, C., Li, C. & Hochholdinger, F. Genetic control of lateral root formation in
922 cereals. *Trends Plant Sci.* **21**, 951–961 (2016).
923 32. Hochholdinger, F., Yu, P. & Marcon, C. Genetic control of root system development in
924 maize. *Trends Plant Sci.* **23**, 79–88 (2018).
925 33. Finkel, O. M. et al. A single bacterial genus maintains root development in a complex
926 microbiome. *Nature* **587**, 103–108 (2020).
927 34. Zhang, J. et al. NRT1.1B is associated with root microbiota composition and nitrogen use
928 in field-grown rice. *Nat. Biotechnol.* **37**, 676–684 (2019).
929 35. Szoboszlay, M., Lambers, J., Chappell, J., Kupper, J. V., Moe, L. A. & McNear Jr, D. H.
930 Comparison of root system architecture and rhizosphere microbial communities of Balsas
931 teosinte and domesticated corn cultivars. *Soil Biol. Biochem.* **80**, 34–44 (2015).
932 36. Brisson, V. L., Schmidt, J. E., Northen, T. R., Vogel, J. P. & Gaudin, A. Impacts of maize
933 domestication and breeding on rhizosphere microbial community recruitment from a
934 nutrient depleted agricultural soil. *Sci. Rep.* **9**, 1–14 (2019).
935 37. Wagner, M. R., Roberts, J. H., Balint-Kurti, P. & Holland, J. B. Heterosis of leaf and
936 rhizosphere microbiomes in field-grown maize. *New Phytol.* **228**, 1055–1069 (2020).
937 38. Favela, A., Bohn, M. O. & Kent, A. D. Maize germplasm chronosequence shows crop
938 breeding history impacts recruitment of the rhizosphere microbiome. *ISME J.* **15**, 2454–
939 2464 (2021).
940 39. Pérez-Jaramillo, J. E., Mendes, R. & Raaijmakers, J. M. Impact of plant domestication on
941 rhizosphere microbiome assembly and functions. *Plant Mol. Biol.* **90**, 635–644 (2016).
942 40. Wagner, M. R. et al. Microbe-dependent heterosis in maize. *Proc. Natl Acad. Sci. USA* **118**,
943 e2021965118 (2021).

Supplementary references

41. Baldauf, J. A. et al. Single-parent expression is a general mechanism driving extensive complementation of non-syntenic genes in maize hybrids. *Curr. Biol.* **28**, 431–437 (2018).
42. Rueda-Ayala, V., Ahrends, H. E., Siebert, S., Gaiser, T., Hüging, H. & Ewert, F. Impact of nutrient supply on the expression of genetic improvements of cereals and row crops–A case study using data from a long-term fertilization experiment in Germany. *Eur. J. Agron.* **96**, 34–46 (2018).
43. Lasky, J. R. et al. Genome-environment associations in sorghum landraces predict adaptive traits. *Sci. Adv.* **1**, e1400218 (2015).
44. Zomer, R. J., Trabucco, A., Bossio, D. A. & Verchot, L. V. Climate change mitigation: A spatial analysis of global land suitability for clean development mechanism afforestation and reforestation. *Agric. Ecosyst. Environ.* **126**, 67–80 (2008).
45. Kalnay, E. et al. The NCEP/NCAR 40-year reanalysis project. *Bull. Am. Meteorol. Soc.* **77**, 437–472 (1996).
46. New, M., Lister, D., Hulme, M. & Makin, I. A high-resolution data set of surface climate over global land areas. *Clim. Res.* **21**, 1–25 (2002).
47. Hengl, T. et al. SoilGrids250m: Global gridded soil information based on machine learning. *PLoS One* **12**, e0169748 (2017).
48. Shangguan, W., Dai, Y., Duan, Q., Liu, B. & Yuan, H. A global soil data set for earth system modeling. *J. Adv. Model. Earth Syst.* **6**, 249–263 (2014).
49. Caporaso, J. G. et al. Global patterns of 16S rRNA diversity at a depth of millions of sequences per sample. *Proc. Natl Acad. Sci. USA* **108**, 4516–4522 (2011).
50. Magoč, T. & Salzberg, S. L. FLASH: fast length adjustment of short reads to improve genome assemblies. *Bioinformatics* **27**, 2957–2963 (2011).
51. Bolyen, E. et al. Reproducible, interactive, scalable and extensible microbiome data science using QIIME 2. *Nat. Biotechnol.* **37**, 852–857 (2019).
52. Callahan, B. J. et al. DADA2: High-resolution sample inference from Illumina amplicon data. *Nat. Methods* **13**, 581–583 (2016).
53. Bokulich, N. A. et al. Optimizing taxonomic classification of marker-gene amplicon sequences with QIIME 2's q2-feature-classifier plugin. *Microbiome* **6**, 1–17 (2018).
54. Yilmaz, P. et al. The SILVA and "all-species living tree project (LTP)" taxonomic frameworks. *Nucleic Acids Res.* **42**, D643–D648 (2014).
55. Katoh, K., Misawa, K., Kuma, K. I. & Miyata, T. MAFFT: a novel method for rapid multiple sequence alignment based on fast Fourier transform. *Nucleic Acids Res.* **30**, 3059–3066 (2002).
56. Price, M. N., Dehal, P. S. & Arkin, A. P. FastTree 2–approximately maximum-likelihood trees for large alignments. *PloS One* **5**, p.e9490 (2010).
57. Abarenkov, Kessy; Zirk, Allan; Piirmann, Timo; Pöhönen, Raivo; Ivanov, Filipp; Nilsson, R. Henrik; Kõljalg, Urmas (2021): UNITE QIIME release for Fungi. Version 10.05.2021. UNITE Community.
58. R Core Team (2021). R: A language and environment for statistical computing. R Foundation for Statistical Computing, Vienna, Austria. URL https://www.R-project.org/.
59. Love, M. I., Huber, W. & Anders, S. Moderated estimation of fold change and dispersion for RNA-seq data with DESeq2. *Genome Biol*. **15**, 550 (2014).
60. Oksanen, J. et al. (2020). vegan: Community Ecology Package. R package version 2.5-7. https://CRAN.R-project.org/package=vegan
61. Kurtz, Z. D., Müller, C. L., Miraldi, E. R., Littman, D. R., Blaser, M. J. & Bonneau, R. A. Sparse and compositionally robust inference of microbial ecological networks. *PLoS Comput. Biol.* **11**, p.e1004226 (2015).
62. Meinshausen, N. & Bühlmann, P. High dimensional graphs and variable selection with the Lasso. *Ann. Stat.* **34**, 1436–1462 (2006).
63. Guo, Z. et al. Development of multiple SNP marker panels affordable to breeders through genotyping by target sequencing (GBTS) in maize. *Mol. Breed.* **39**,1–12 (2019).
64. Rogers, J. S. (1972). Measures of similarity and genetic distance. In Studies in Genetics VII. pp. 145−153. University of Texas Publication 7213. Austin, Texas
65. Yang, J., Lee, S. H., Goddard, M. E. & Visscher, P. M. GCTA: a tool for genome-wide complex trait analysis. *Am. J. Hum. Genet.* **88**, 76–82 (2011).
66. Kumar, S., Stecher, G., Li, M., Knyaz, C. & Tamura, K. MEGA X: molecular evolutionary genetics analysis across computing platforms. *Mol. Biol. Evol.* **35**, 1547 (2018).

67. Bernal-Vasquez, A. M., Utz, H. F. & Piepho, H. P. Outlier detection methods for generalized lattices: a case study on the transition from ANOVA to REML. *Theor. Appl. Genet.* **129**, 787–804 (2016).
68. Butler, D. G., Cullis, B. R., Gilmour A. R., Gogel, B. G. & Thompson, R. ASReml-R Reference Manual Version 4. (2017) VSN International Ltd, Hemel Hempstead, HP1 1ES, UK.
69. Browning, B. L., Zhou, Y. & Browning, S. R. A one-penny imputed genome from next generation reference panels. *Am. J. Hum. Genet.* **103**, 338–348 (2018).
70. Yu, J. et al. A unified mixed-model method for association mapping that accounts for multiple levels of relatedness. *Nat. Genet.* **38**, 203–208 (2006).
71. VanRaden, P. M. Efficient methods to compute genomic predictions. *J. Dairy Sci.* **91**, 4414–4423 (2008).
72. Zhang, Z. et al. Mixed linear model approach adapted for genome-wide association studies. *Nat. Genet.* **42**, 355–360 (2010).
73. Pérez, P. & de Los Campos. G. Genome-wide regression and prediction with the BGLR statistical package. *Genetics* **198**, 483–495 (2014).
74. Holm, S. A simple sequentially rejective multiple test procedure. *Scand. J. Stat.* **6**, 65–70 (1979).
75. Benjamini, Y. & Hochberg, Y. Controlling the false discovery rate: a practical and powerful approach to multiple testing. *J. Royal Stat. Soc. Ser. B.* **57**, 289–300 (1995).
76. Chen, H. et al. Control for population structure and relatedness for binary traits in genetic association studies via logistic mixed models. *Am. J. Hum. Genet.* **98**, 653–666 (2016).
77. Breslow, N. E. & Clayton, D. G. Approximate inference in generalized linear mixed models. *J. Am. Stat. Assoc.* **88**, 9–25 (1993).
78. Efron, B. Bootstrap methods: another look at the jackknife. *Ann. Stat.* **7**, 1–26 (1979).
79. Schmitz Carley, C. A. et al. Automated tetraploid genotype calling by hierarchical clustering. *Theor. Appl. Genet.* **130**, 717–726 (2017).
80. de Cáceres, M., Jansen, F. & Dell, N. Indicspecies: Relationship between species and groups of sites, R package (2020).
81. Kursa, M. B. & Rudnicki, W. R. Feature selection with the Boruta package. *J. Stat. Softw.* **36**, 1–13 (2010).
82. Liaw, A. & Wiener, M. Classification and regression by randomForest. *R news* **2**, 18–22 (2002).
83. Gates, D. J. et al. Single-gene resolution of locally adaptive genetic variation in Mexican maize. *Preprint at bioRxiv* https://doi.org/10.1101/706739 (2019).
84. François, O., Martins, H., Caye, K. & Schoville, S. D. Controlling false discoveries in genome scans for selection. *Mol. Ecol.* **25**, 454–469 (2016).
85. Marcon, C. et al. BonnMu: a sequence-indexed resource of transposon-induced maize mutations for functional genomics studies. *Plant Physiol.* **184**, 620–631 (2020).
86. Bates, D., Mächler, M., Bolker, B., & Walker, S. Fitting linear mixed-effects models using lme4. *J. Stat. Softw.* **67**, 1–48 (2015).